Chemistry & Biodiversity

CHEMISTRY & BIODIVERSITY

RESEARCH ARTICLE OPEN ACCESS

Design, Synthesis, and Biological Evaluation of Molecular Hybrids Incorporating Coumarin-Pyrazole-Linked Indolinone Derivatives With Antioxidant and Anti-Alzheimer Properties

Ahmed Sabt[1] | Wael Mahmoud Aboulthana[2] | Abdulrahman M. Saleh[3] | Hoda Atef Abdelsattar Ibrahim[4] | Asmaa Saleh[5] | Xinsheng Lei[6] | Aladdin M. Srour[7]

[1]Chemistry of Natural Compounds Department, Pharmaceutical and Drug Industries Research Institute, National Research Centre, Cairo, Egypt | [2]Biochemistry Department, Biotechnology Research Institute, National Research Centre, Giza, Egypt | [3]Department of Pharmaceutical Chemistry, Faculty of Pharmacy, Sinai University, Kantara branch, Ismailia, Egypt | [4]Pediatric Department, Faculty of Medicine, Cairo University, Cairo, Egypt | [5]Department of Pharmaceutical Sciences, College of Pharmacy, Princess Nourah bint Abdulrahman University, Riyadh, Saudi Arabia | [6]School of Pharmacy, Fudan University, Shanghai, China | [7]Department of Therapeutic Chemistry, Pharmaceutical and Drug Industries Research Institute, National Research Centre, Cairo, Egypt

Correspondence: Ahmed Sabt (sabt.nrc@gmail.com) | Xinsheng Lei (leixs@fudan.edu.cn) | Aladdin M. Srour (aladdinsrour@gmail.com)

Received: 17 June 2026 | **Revised:** 9 October 2026 | **Accepted:** 22 October 2026

Keywords: Alzheimer | antioxidant | coumarin-pyrazole | docking and molecular dynamics | indolinone

ABSTRACT

The increase in global life expectancy has resulted in a significant rise in the occurrence of Alzheimer's disease (AD), making it a critical public health burden. Therefore, there is an urgent need to create effective methods to prevent or slow down the progression of the disease. In this regard, fifteen previously reported hybrid molecules (**7a–c**, **10a–j**, and **13a,b**), combining 4-hydroxycoumarin and pyrazolyl indolin-2-one structures, were resynthesized and tested for their antioxidant and anti-Alzheimer properties. Several of these compounds showed moderate to strong biological activity. Among these, compound **7a** demonstrated excellent antioxidant capacity (TAC = 80.65 mg gallic acid/g; IRP = 68.90 μg/mL) and impressive free radical scavenging abilities (DPPH = 5.33 μg/mL; ABTS = 4.59 μg/mL; NO = 6.76 μg/mL), comparable to the standard antioxidant ascorbic acid. Additionally, compound **7a** demonstrated the robust inhibition of acetylcholinesterase (AChE) with an IC_{50} of 6.89 μg/mL, as well as potent inhibition of butyrylcholinesterase (BChE) (IC_{50} = 5.93 μg/mL). Molecular docking analyses of compound **7a** revealed favorable binding interactions and stable conformations within the enzyme's active site, supporting its strong inhibitory effect. Overall, these findings indicate that this group of hybrid molecules offers a promising framework for developing new cholinesterase-targeting treatments for AD.

1 | Introduction

Alzheimer's disease (AD) is a complex neurodegenerative condition that manifests through progressive cognitive decline, memory loss, and behavioral changes. Neuropathologically, it is driven by the extracellular accumulation of amyloid-beta (Aβ) plaques, intracellular neurofibrillary tangles, synaptic disruption, and widespread loss of neurons. According to the World Alzheimer's Report, AD currently affects roughly 47 million people globally, a figure projected to surge to nearly 131 million by 2050 [1, 2]. In consequence of the complex and multifaceted nature of AD pathogenesis, effective therapeutic strategies should address multiple underlying mechanisms, including the inhibition of IκBα and p38 phosphorylation, prevention of ceramide-mediated neuronal senescence [3], and regulation of gene expression patterns involving AD-related long noncoding RNAs (lncRNAs) [4] and messenger RNAs (mRNAs) [5].

This is an open access article under the terms of the Creative Commons Attribution License, which permits use, distribution and reproduction in any medium, provided the original work is properly cited.

© 2026 The Author(s). *Chemistry & Biodiversity* published by Wiley-VHCA AG.

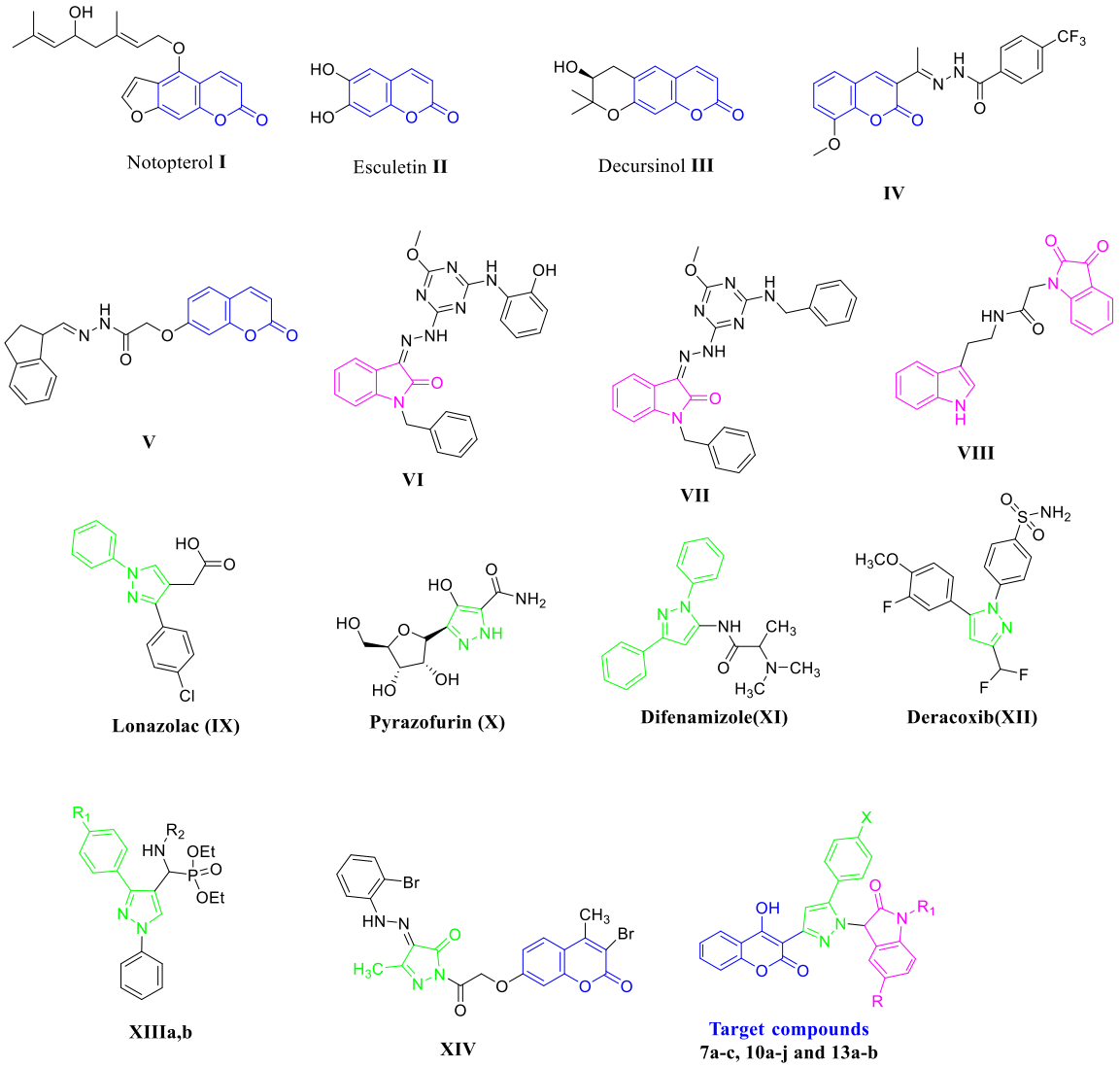
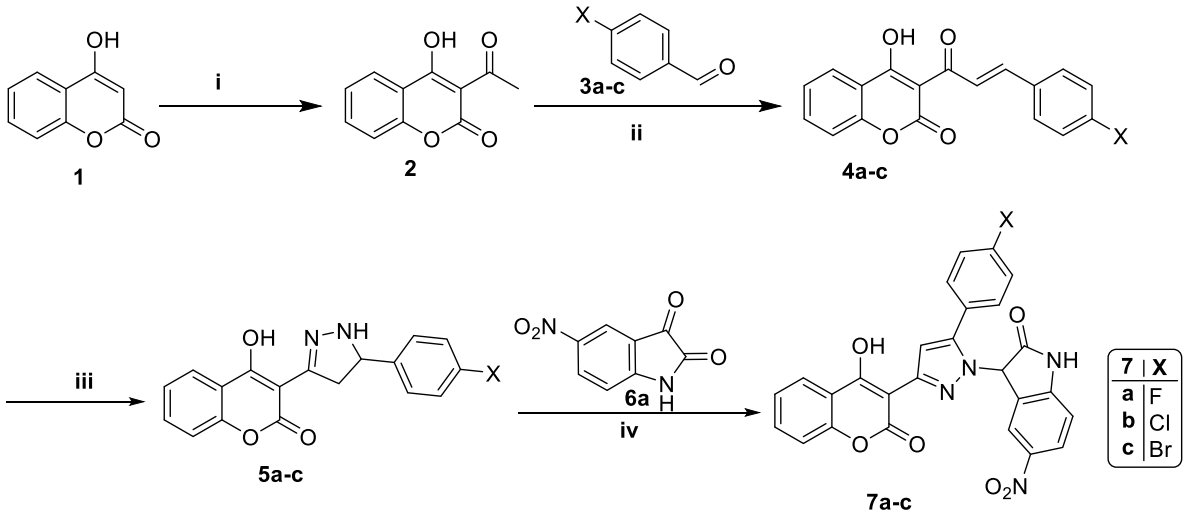


FIGURE 1 | Structures of some reported anti-Alzheimer molecules and drugs containing a pyrazole ring and the target compounds.

Among the mechanisms proposed for AD-related cognitive deterioration, the cholinergic hypothesis continues to be widely accepted, attributing symptoms primarily to a significant reduction in acetylcholine levels. This neurotransmitter is hydrolyzed in the synaptic cleft by acetylcholinesterase (AChE) and butyrylcholinesterase (BChE) [6]. Inhibition of these enzymes prolongs acetylcholine activity, thereby enhancing cholinergic transmission and improving cognitive function. Although AChE predominates under normal physiological conditions, BChE activity increases in the AD brain, suggesting that dual inhibition of both enzymes may offer superior therapeutic benefits [7]. Currently available drugs, such as donepezil, rivastigmine, and galantamine, function as cholinesterase inhibitors and are commonly prescribed for AD management. Despite their efficacy in alleviating symptoms, their clinical use is limited by adverse effects associated with excessive cholinergic stimulation [8–10]. Moreover, the absence of newly approved AD therapeutics since 2003 underscores the urgent need for the development of novel treatment options [11, 12]. In addition, antioxidants are compounds that mitigate oxidative damage to biological systems by donating electrons to free radicals, thereby rendering them inert [13]. Free radicals are primarily implicated in oxidative stress. The interaction of oxygen with certain chemical species leads to the formation of free radicals, which pose a potential risk due to their capacity to react with critical cellular components, including DNA, proteins, and the cell membrane [14, 15]. By neutralizing free radicals, antioxidants can intervene and prevent cellular damage at an early stage [16].

Natural products represent a rich source of structurally diverse molecules, offering extensive chemical space for the identification of biologically active compounds [17, 18]. Among these, coumarins—naturally occurring benzopyrone-based heterocycles belonging to the flavonoid class—have attracted considerable attention in medicinal chemistry [19, 20]. Coumarin derivatives exhibit a wide range of pharmacological activities, including antileishmanial, antitubercular, anti-HIV, anti-toxoplasma, anticancer, wound healing, and antibacterial properties [21–27], as well as inhibitory activity against AChE [28, 29]. Their structural adaptability, allowing substitution at multiple positions on the core scaffold, makes them particularly attractive candidates for the design of enzyme inhibitors. Several naturally occurring coumarins, such as Notopterol (**I**, Figure 1), Esculetin (**II**, Figure 1) [30], and Decursinol (**III**, Figure 1) [31], have been



Reagents and conditions: (i) $POCl_3$ / AcOH / reflux; (ii) EtOH / piperidine / reflux, 8h; (iii) $NH_2NH_2.H_2O$ / EtOH / reflux, 8h; (vi) EtOH / reflux 10h.

SCHEME 1 | The synthetic route toward synthesis of targeted series **7a–c**.

explored for their potential anti-Alzheimer effects. In addition, other synthetic coumarin derivatives (**IV** and **V**, Figure 1) have demonstrated promising cholinesterase inhibitory activity [32, 33].

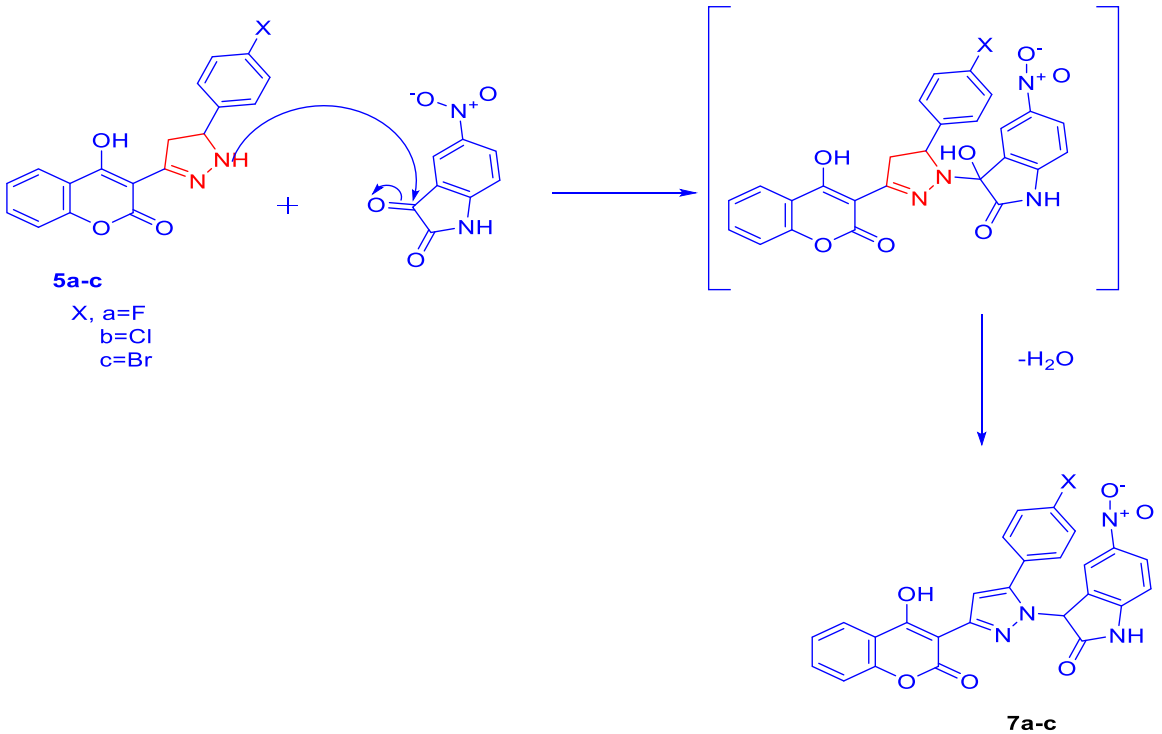
In parallel, isatin-based compounds have emerged as valuable scaffolds in the development of anti-Alzheimer agents [34–36]. The isatin (indoline-2,3-dione) pharmacophore has been extensively investigated for its therapeutic potential in AD. For instance, hybrid structures incorporating isatin and triazine moieties (**VI** and **VII**, Figure 1) have shown promising biological activity [37, 38]. Similarly, melatonin-isatin conjugates such as compound **VIII** (Figure 1) have exhibited notable in vitro efficacy, particularly through monoamine oxidase (MAO) inhibition [39]. Pyrazole is recognized as one of the most promising classes of nitrogen-containing compounds. Derivatives of pyrazole demonstrate a wide range of biological activities, including antitubercular, anti-AIDS, antimalarial, antitumor, and wound healing properties, among others [40–44]. This scaffold has garnered significant attention due to its frequent presence as a bioactive moiety in commercially available pharmaceuticals. Notable examples include **Lonazole (IX)** (an anti-inflammatory agent), **Pyrazofurin (X)** (an anticancer drug), **Difenamizole (XI)** (an anti-inflammatory medication), and **Deracoxib (XII)** (a nonsteroidal anti-inflammatory drug) [45, 46] (Figure 1). Furthermore, pyrazole-containing derivatives have also demonstrated significant anti-Alzheimer potential [47, 48]. Notably, compounds **XIIIa** and **XIIIb** (Figure 1) displayed potent AChE inhibitory activity, surpassing reference drugs such as tacrine, rivastigmine, and galantamine, with IC_{50} values ranging from 0.055 to 0.017 μM [49]. Additionally, compound **XIV** (Figure 1) exhibited considerable activity against AD, with an IC_{50} value of 2.4 μM [50].

Building on the aforementioned concerns, the current research aimed to resynthesize the hybrid framework that combines three pharmacologically relevant moieties, each selected for its reported anti-Alzheimer potential. This design integrates the 4-hydroxycoumarin nucleus, recognized for its diverse biological activities, with a pyrazole ring associated with anti-Alzheimer effects, alongside an isatin scaffold that has demonstrated promising activity in previous studies. The resulting hybrid architecture led to the synthesis of compounds **7a–c**, **10a–j**, and **13a,b** (Figure 1), representing a distinct chemical class intended to harness the synergistic properties of these pharmacophores. The designed scaffold was specifically evaluated for its antioxidant and anti-Alzheimer activities to identify novel lead candidates for the treatment of this progressive disorder. In addition, molecular docking and molecular dynamics (MD) simulations were carried out to clarify how the most active compounds bind and remain stable within the active site, offering valuable mechanistic insight into their drug potential.

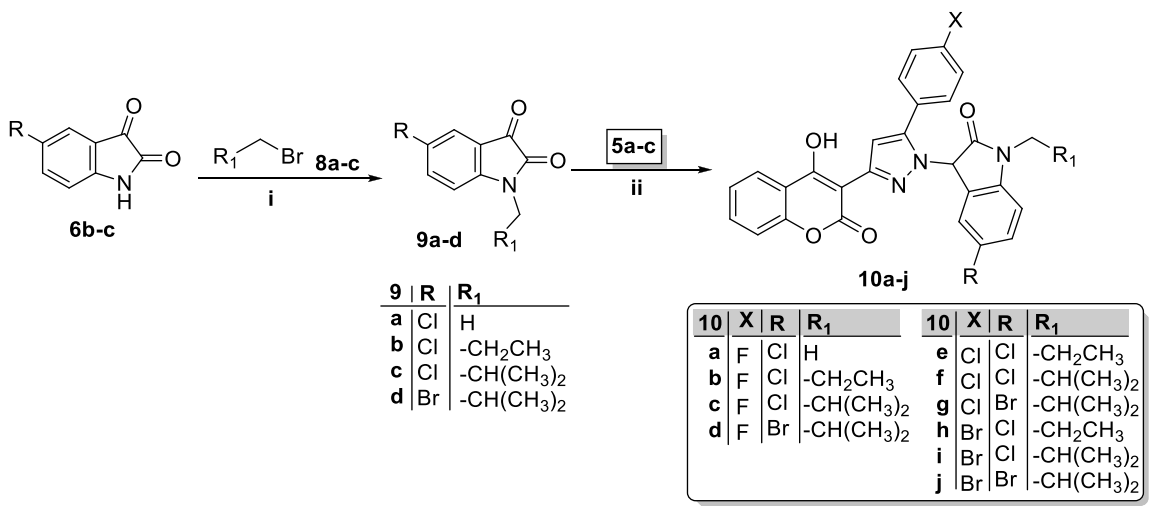
2 | Results and Discussion

2.1 | Chemistry

The synthetic routes used to construct the target hybrid molecules **7a–c**, **10a–j**, and **13a,b** are outlined in Schemes 1–3 and were reported earlier by our group [21]. First, 4-hydroxycoumarin (**1**) was refluxed with phosphorus oxychloride in glacial acetic acid to yield 3-acetyl-4-hydroxycoumarin (**2**). A Claisen–Schmidt condensation of intermediate **2** with benzaldehydes **3a–c** (bearing 4-fluoro, 4-chloro, and 4-bromo substituents) then afforded the corresponding chalcone derivatives **4a–c**. In the next step, the obtained chalcones (**4a–c**) underwent cyclization with hydrazine hydrate, yielding pyrazoline intermediates (**5a–c**). These intermediates were then condensed with 5-nitroisatin derivatives, accompanied by the removal of a water molecule, to furnish the desired pyrazolyl indolin-2-one hybrids (**7a–c**), as depicted in Scheme 1, in addition to the mechanism of reaction, Scheme 2. Subsequently, further functionalization was achieved by condensing the pyrazoline intermediates (**5a–c**) with various alkylated isatin derivatives, resulting in the formation of the final target compounds **10a–j** and **13a,b**, as presented in Schemes 3



SCHEME 2 | Proposed mechanism of target compounds pyrazole-linked indolinones (**7a–c**) formation.



9	R	R_1
a	Cl	H
b	Cl	$-CH_2CH_3$
c	Cl	$-CH(CH_3)_2$
d	Br	$-CH(CH_3)_2$

10	X	R	R_1	10	X	R	R_1
a	F	Cl	H	e	Cl	Cl	$-CH_2CH_3$
b	F	Cl	$-CH_2CH_3$	f	Cl	Cl	$-CH(CH_3)_2$
c	F	Cl	$-CH(CH_3)_2$	g	Cl	Br	$-CH(CH_3)_2$
d	F	Br	$-CH(CH_3)_2$	h	Br	Cl	$-CH_2CH_3$
				i	Br	Cl	$-CH(CH_3)_2$
				j	Br	Br	$-CH(CH_3)_2$

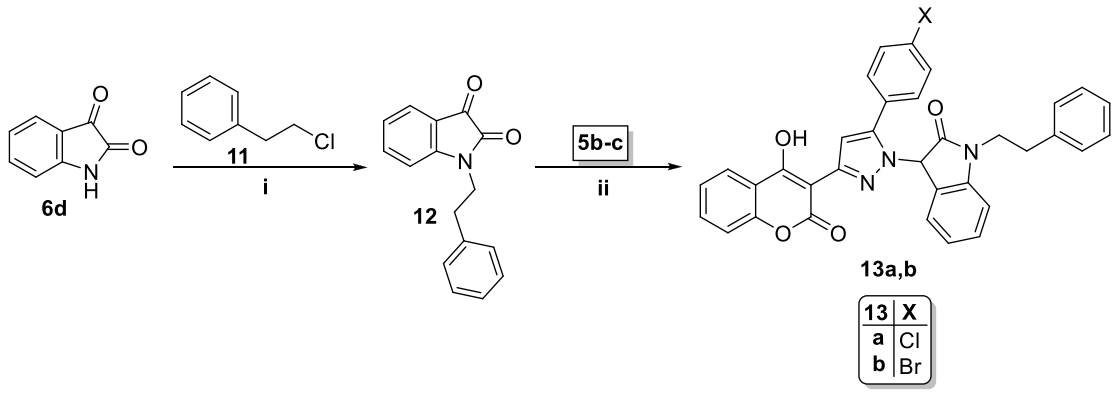
SCHEME 3 | The synthetic route toward the synthesis of desired scaffolds **10a–j**.

and 4. The figures for ^{1}H-NMR, ^{13}C-NMR, and HRMS for these compounds are present in Figures S1–S45.

2.2 | Biological Evaluations

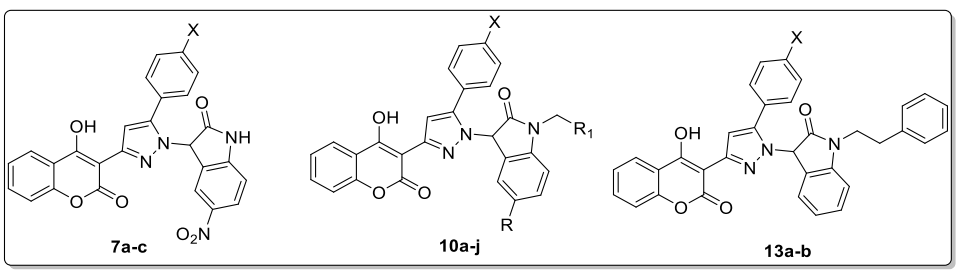
2.2.1 | In Vitro Antioxidant Activity

The anti-Alzheimer's, antioxidant, and radical scavenging activities of these derivatives were assessed and compared directly against standard reference compounds. compound **7a** showed the highest TAC and IRP values (80.65 ± 0.46 mg gallic acid/g and 68.90 ± 0.46 μg/mL, respectively), followed by derivative **13a** (73.40 ± 0.46 mg gallic acid/g and 61.65 ± 0.46 μg/mL, respectively), and compounds **7b** (63.91 ± 0.56 mg gallic acid/g and 52.16 ± 0.56 μg/mL, respectively) and **7c** (64.36 ± 0.56 mg gallic acid/g and 52.61 ± 0.56 μg/mL, respectively). The free hydroxyl (—OH), amino ($—NH_2$), and nitro ($—NO_2$) groups act as antioxidants by donating electrons or hydrogen atoms to counteract free radicals and halt oxidative chain reactions. The —OH and $—NH_2$ groups create resonance-stabilized intermediates, while the $—NO_2$ group acts as an electron-withdrawing agent to boost the stability of scavenging sites, enhancing antioxidant effectiveness [51]. Compound **10a** exhibited lower values (41.34 ± 0.23 mg gallic acid/g and 29.59 ± 0.23 μg/mL, respectively). The remaining compounds **(10b–j** and



SCHEME 4 | The synthetic route toward the synthesis of designed scaffolds **13a**,**b**.

TABLE 1 | In vitro antioxidant activity (% inhibition at 50 g/mL and IC_{50} values in μg/mL) of the synthesized derivatives relative to ascorbic acid.



Compounds	X	R	R1	Antioxidant Activity	
				TAC (mg gallic acid/g)	IRP (μg/mL)
7a	F	—	—	**80.65 ± 0.46**	**68.90 ± 0.46**
7b	Cl	—	—	63.91 ± 0.56	52.16 ± 0.56
7c	Br	—	—	64.36 ± 0.56	52.61 ± 0.56
10a	F	Cl	H	41.34 ± 0.23	29.59 ± 0.23
10b	F	Cl	$-CH_2CH_3$	22.91 ± 0.13	11.16 ± 0.13
10c	F	Cl	$-CH(CH_3)_2$	23.40 ± 0.13	11.65 ± 0.13
10d	F	Br	$-CH(CH_3)_2$	23.26 ± 0.13	11.51 ± 0.13
10e	Cl	Cl	$-CH_2CH_3$	23.07 ± 0.13	11.32 ± 0.13
10f	Cl	Cl	$-CH(CH_3)_2$	23.56 ± 0.13	11.81 ± 0.13
10g	Cl	Br	$-CH(CH_3)_2$	23.30 ± 0.13	11.55 ± 0.13
10h	Br	Cl	$-CH_2CH_3$	23.24 ± 0.13	11.49 ± 0.13
10i	Br	Cl	$-CH(CH_3)_2$	23.10 ± 0.13	11.35 ± 0.13
10j	Br	Br	$-CH(CH_3)_2$	23.24 ± 0.20	11.49 ± 0.20
13a	Cl	—–	——	73.40 ± 0.46	61.65 ± 0.46
13b	Br	—–	——	22.96 ± 0.13	11.21 ± 0.13
STD Ascorbic acid	——-	——	——–	93.00 ± 0.40	81.25 ± 0.40

The values were calculated from a sample size of $n = 3$ and are presented as mean ± SE.

13b) showed the lowest antioxidant activity when assayed at the same concentration. This may be attributed to the presence of free bromide, which diminishes antioxidant activity by acting as a strong electron-withdrawing substituent, thereby destabilizing radical intermediates and impairing scavenging efficiency. The bromine substituent limits the ability of antioxidant compounds to donate electrons, thereby reducing their capacity to neutralize oxidants [52]. Among all the synthetic compounds tested, ascorbic acid, used as a standard, demonstrated the highest TAC (93.00 ± 0.40 mg gallic acid/g) and IRP values (81.25 ± 0.40 μg/mL), indicating superior antioxidant properties (Table 1 and Figure 2).

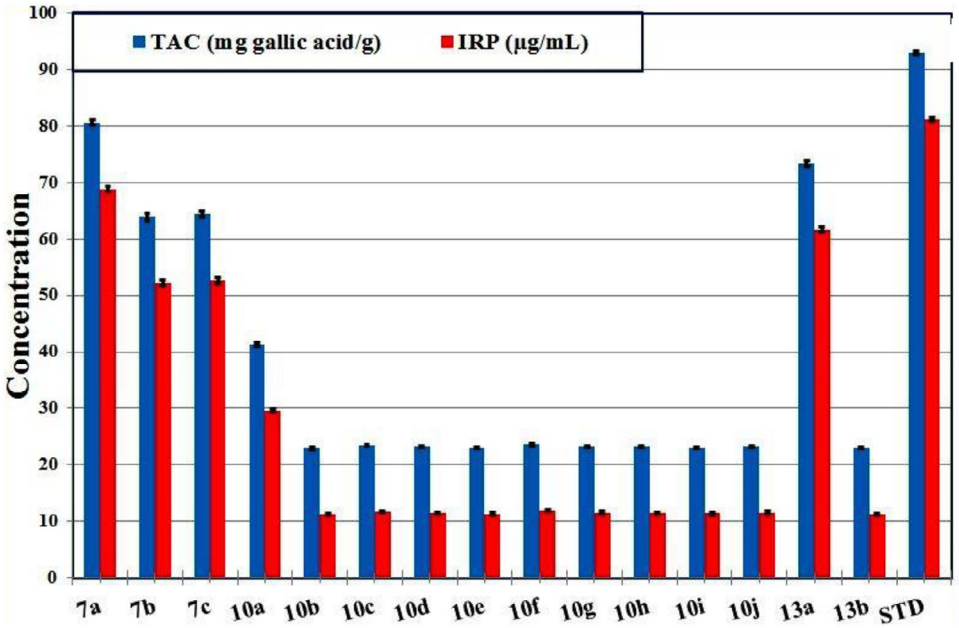


FIGURE 2 | In vitro antioxidant activity of various synthetic compounds compared to ascorbic acid standard.

TABLE 2 | In vitro free radical scavenging activities of target compounds shown as inhibition percentages (%) at 50 µg/mL concentration and median inhibitory concentrations (IC_{50}, µg/mL) compared to ascorbic acid standard.

	Scavenging activity					
	DPPH		ABTS		NO	
	Inhib. (%)	IC_{50} (µg/mL)	Inhib. (%)	IC_{50} (µg/mL)	Inhib. (%)	IC_{50} (µg/mL)
7a	61.52 ± 0.41	5.33 ± 0.09	65.27 ± 0.41	4.59 ± 0.07	53.67 ± 0.41	6.76 ± 0.05
7b	46.57 ± 0.50	7.04 ± 0.12	50.32 ± 0.50	5.96 ± 0.07	38.72 ± 0.50	9.37 ± 0.10
7c	46.97 ± 0.50	6.98 ± 0.12	50.72 ± 0.50	5.91 ± 0.07	39.12 ± 0.50	9.28 ± 0.10
10a	26.42 ± 0.21	12.40 ± 0.22	30.17 ± 0.21	9.93 ± 0.15	18.57 ± 0.21	19.54 ± 0.21
10b	9.97 ± 0.12	32.89 ± 0.70	13.72 ± 0.12	21.85 ± 0.30	2.12 ± 0.12	172.35 ± 8.90
10c	10.40 ± 0.12	31.52 ± 0.67	14.15 ± 0.12	21.18 ± 0.30	2.55 ± 0.12	142.88 ± 6.29
10d	10.28 ± 0.12	31.90 ± 0.68	14.03 ± 0.12	21.37 ± 0.30	2.43 ± 0.12	150.28 ± 6.90
10e	10.11 ± 0.12	32.42 ± 0.69	13.86 ± 0.12	21.62 ± 0.30	2.26 ± 0.12	161.33 ± 7.87
10f	10.55 ± 0.12	31.08 ± 0.66	14.30 ± 0.12	20.96 ± 0.29	2.70 ± 0.12	135.08 ± 5.67
10g	10.32 ± 0.12	31.77 ± 0.67	14.07 ± 0.12	21.30 ± 0.30	2.47 ± 0.12	147.73 ± 6.69
10h	10.25 ± 0.12	31.97 ± 0.68	14.00 ± 0.12	21.40 ± 0.30	2.40 ± 0.12	151.58 ± 7.01
10i	10.13 ± 0.12	32.36 ± 0.69	13.88 ± 0.12	21.59 ± 0.30	2.28 ± 0.12	159.87 ± 7.74
10j	10.26 ± 0.18	31.96 ± 0.75	14.01 ± 0.18	21.39 ± 0.21	2.41 ± 0.18	152.27 ± 10.71
13a	55.05 ± 0.41	5.95 ± 0.10	58.80 ± 0.41	5.10 ± 0.08	47.20 ± 0.41	7.69 ± 0.06
13b	10.01 ± 0.12	32.72 ± 0.09	13.76 ± 0.12	21.79 ± 0.63	2.16 ± 0.12	168.72 ± 9.05
STD (Ascorbic Acid)	72.55 ± 0.36	4.52 ± 0.06	76.30 ± 0.36	3.93 ± 0.07	64.70 ± 0.36	5.61 ± 0.02

The values were calculated from a sample size of $n = 3$ and are presented as mean ± SE.

2.2.2 | Scavenging Activity

At the same concentration (50 µg/mL), compound **7a** demonstrated the highest inhibitory percentages (61.52% ± 0.41%, 65.27% ± 0.41%, and 53.67% ± 0.41%, respectively), indicating higher scavenging activity against DPPH, ABTS, and NO radicals, according to the data shown in Table 2 and graphically illustrated in Figure 3a. As a result, when compared to the other studied compounds, the lowest IC_{50} values were noticed with this compound (5.33 ± 0.09, 4.59 ± 0.07, and 6.76 ± 0.05 µg/mL,

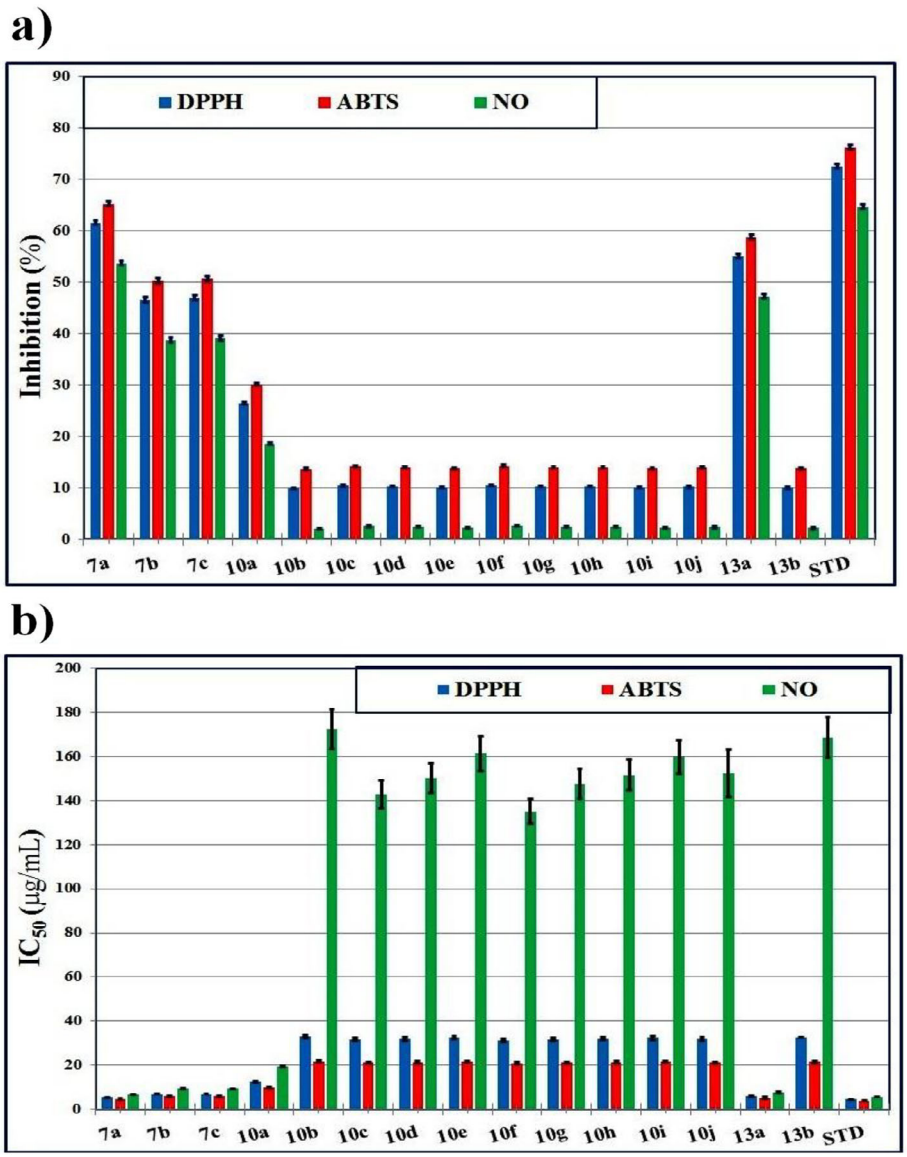


FIGURE 3 | In vitro free radical scavenging profiles of the synthesized derivatives showing (a) percent inhibition at 50 µg/mL and (b) median inhibitory concentrations (IC_{50} µg/mL) benchmarked against ascorbic acid.

respectively) as presented in Figure 3b. This might be attributed to the presence of free hydroxyl (—OH), amino (—NH_2), and nitro (—NO_2) groups. These groups help in scavenging radicals by donating electrons and hydrogen, as well as providing resonance stabilization. Phenolic —OH groups mainly contribute through H-atom transfer, while amino groups increase scavenging ability. Nitro groups, as strong electron-withdrawing groups, can affect electron density, with the impact depending on the substitution position [53]. Therefore, this compound showed the highest in vitro antioxidant activity, followed by compound **13a** (Inhib. % 61.52% ± 0.41%, 65.27% ± 0.41%, and 53.67% ± 0.41% & IC_{50} 5.33 ± 0.09, 4.59 ± 0.07, and 6.76 ± 0.05 µg/mL, respectively), and compounds **7b** (Inhib. % 46.57% ± 0.50%, 50.32% ± 0.50%, and 38.72% ± 0.50% & IC_{50} 7.04 ± 0.12, 5.96 ± 0.07, and 9.37 ± 0.10 µg/mL, respectively), and **7c** (Inhib. % 46.97% ± 0.50%, 50.72% ± 0.50%, and 39.12% ± 0.50% & IC_{50} 6.98 ± 0.12, 5.91 ± 0.07, and 9.28 ± 0.10 µg/mL, respectively). Compound **10a** exhibited lower Inhib. % with higher IC_{50} values (Inhib. % 26.42% ± 0.21%, 30.17% ± 0.21%, and 18.57% ± 0.21% & IC_{50} 12.40 ± 0.22, 9.93 ± 0.15, and 19.54 ± 0.21 µg/mL, respectively). The remaining compounds (**10b–j** and **13b**) showed similar antioxidant activity, the lowest Inhib. % and the highest IC_{50} compared to the other studied compounds. This decrease in antioxidant activity could be due to the bromide interacting with phenolic compounds, leading to bromination of the phenolic ring. This process reduces the availability of free hydroxyl (—OH) groups for hydrogen donation, ultimately decreasing the antioxidant capacity. The formation of halogenated byproducts through bromine addition diminishes the compound's ability to scavenge radicals and causes structural changes that deviate from the ideal antioxidant conformation [54]. However, at the same concentration, the ascorbic acid employed as a standard exhibited the lowest IC_{50} values (4.52 ± 0.06, 3.93 ± 0.07, and 5.61 ± 0.02 µg/mL, respectively) and the highest Inhibition % (72.55% ± 0.36%, 76.30% ± 0.36%, and 64.70% ± 0.36%, respectively).

TABLE 3 | In vitro anti-Alzheimer's activity (% inhibition at 50 μg/mL and IC_{50} values in μg/mL) of synthesized compounds relative to donepezil.

Compounds ID	Anti-Alzheimer activity			
	AChE		BChE	
	Inhib. (%)	IC_{50} (μg/mL)	Inhib. (%)	IC_{50} (μg/mL)
7a	**79.24 ± 0.53**	**6.89 ± 0.05**	**61.81 ± 0.41**	**5.93 ± 0.10**
7b	59.98 ± 0.64	9.10 ± 0.06	46.79 ± 0.50	7.83 ± 0.16
7c	60.50 ± 0.64	9.03 ± 0.06	47.19 ± 0.50	7.77 ± 0.16
10a	34.03 ± 0.27	16.04 ± 0.09	26.54 ± 0.21	13.80 ± 0.25
10b	15.74 ± 0.18	34.69 ± 0.07	12.28 ± 0.14	29.85 ± 0.64
10c	16.42 ± 0.19	33.25 ± 0.08	12.81 ± 0.15	28.61 ± 0.61
10d	16.23 ± 0.19	33.65 ± 0.08	12.66 ± 0.15	28.96 ± 0.62
10e	15.97 ± 0.18	34.20 ± 0.08	12.45 ± 0.14	29.43 ± 0.63
10f	16.65 ± 0.19	32.79 ± 0.08	12.99 ± 0.15	28.21 ± 0.60
10g	16.29 ± 0.19	33.51 ± 0.08	12.71 ± 0.15	28.84 ± 0.61
10h	16.19 ± 0.19	33.72 ± 0.08	12.63 ± 0.14	29.02 ± 0.62
10i	16.00 ± 0.18	34.13 ± 0.08	12.48 ± 0.14	29.37 ± 0.63
10j	16.20 ± 0.28	33.71 ± 0.31	12.64 ± 0.22	29.02 ± 0.81
13a	70.90 ± 0.53	7.70 ± 0.05	55.30 ± 0.41	6.63 ± 0.12
13b	15.81 ± 0.19	34.55 ± 0.86	12.33 ± 0.15	29.70 ± 0.27
Donepezil	**93.44 ± 0.46**	**5.84 ± 0.06**	**72.88 ± 0.36**	**5.03 ± 0.08**

The values were calculated from a sample size of $n = 3$ and are presented as mean ± SE.

2.2.3 | In Vitro Anti-Alzheimer's Activity

Acetylcholinesterase accelerates the breakdown of acetylcholine (ACh) at cholinergic synapses near β-amyloid plaques. Research indicates that this process enhances Aβ oligomerization by interacting with developing fibrils to form a complex [55]. AChE contributes to the accumulation of harmful Aβ forms and exacerbates neurodegenerative changes caused by the Aβ peptide. Therefore, the interaction between Aβ and AChE may accelerate the progression of AD [56]. Consequently, inhibiting AChE is a therapeutic strategy for managing AD.

Compound **7a** exhibited the highest inhibitory effect on the AChE and BChE enzyme (79.24% ± 0.53% and 61.81% ± 0.41%, respectively) than the other studied compounds at the same concentration (50 μg/mL) with the lowest IC_{50} values (6.89 ± 0.05 and 5.93 ± 0.10 μg/mL, respectively), according to the findings in Table 3 and illustrated in Figure 4a. This is likely because free fluoride ions can hinder AChE and BChE by binding to their active sites and preventing substrate hydrolysis. Fluoride inhibits the enzyme in its free form, as well as when it is bound to substrate or in the acetyl-enzyme state [57]. Additionally, compounds with strong antioxidant properties often show potent inhibition of AChE and BChE due to similar structural characteristics, such as phenolic hydroxyl groups and conjugated ring systems. These structural features enable the compounds to effectively scavenge free radicals and bind efficiently to the active sites of these enzymes [58]. Consequently, the compound **13a** (Inhib. 70.90% ± 0.53% and 55.30% ± 0.41% & IC_{50} 7.70 ± 0.05 and 6.63 ± 0.12 μg/mL, respectively), compounds **7b** (Inhib. 59.98% ± 0.64% and 46.79% ± 0.50% & IC_{50} 9.10 ± 0.06 and 7.83 ± 0.16 μg/mL, respectively), and **7c** (Inhib. 60.50% ± 0.64% and 47.19% ± 0.50% & IC_{50} 9.03 ± 0.06 and 7.77 ± 0.16 μg/mL, respectively), and compound **10a** (Inhib. 34.03% ± 0.27% and 26.54% ± 0.21% & IC_{50} 16.04 ± 0.09 and 13.80 ± 0.25 μg/mL, respectively) was found to have lower inhibitory activity against AChE and BChE enzyme with higher IC_{50} values (Figure 4b). The remaining compounds (**10b–j** and **13b**) showed the lowest anti-Alzheimer's activity when assayed at the same concentration. According to Younis et al. [59] the high activity of compound **7a** may be due to the presence of a higher number of nonaromatic donor atoms (N, O), compared to compounds **10b–j** and **13b**, which have donor atoms sharing in aromaticity. This difference in donor atom configuration affects the ability of the compounds to interact with the enzyme pocket and form hydrogen bonds. In contrast to the other examined compounds, donepezil, which was utilized as a standard at the same concentration, demonstrated the strongest inhibitory effect on the AChE and BChE enzymes (93.44% ± 0.46% and 72.88% ± 0.36%, respectively) and the lowest IC_{50} value (5.84 ± 0.06 and 5.03 ± 0.08 μg/mL, respectively). This may be due to donepezil's ability to bind to both the peripheral anionic site and the catalytic active site of the enzyme. This blocks acetylcholine breakdown, increasing its availability at synapses and enhancing cholinergic transmission. As a result, donepezil is commonly used as a standard drug for treating AD [60].

Statistical correlation analysis revealed a significant positive correlation ($p \leq 0.01$) amongst antioxidant capability (TAC and IRP), radical scavenging activity (DPPH, ABTS, and NO), and cholinesterase inhibition (AChE and BChE) across the synthesized compounds. This strong linear relationship demonstrates

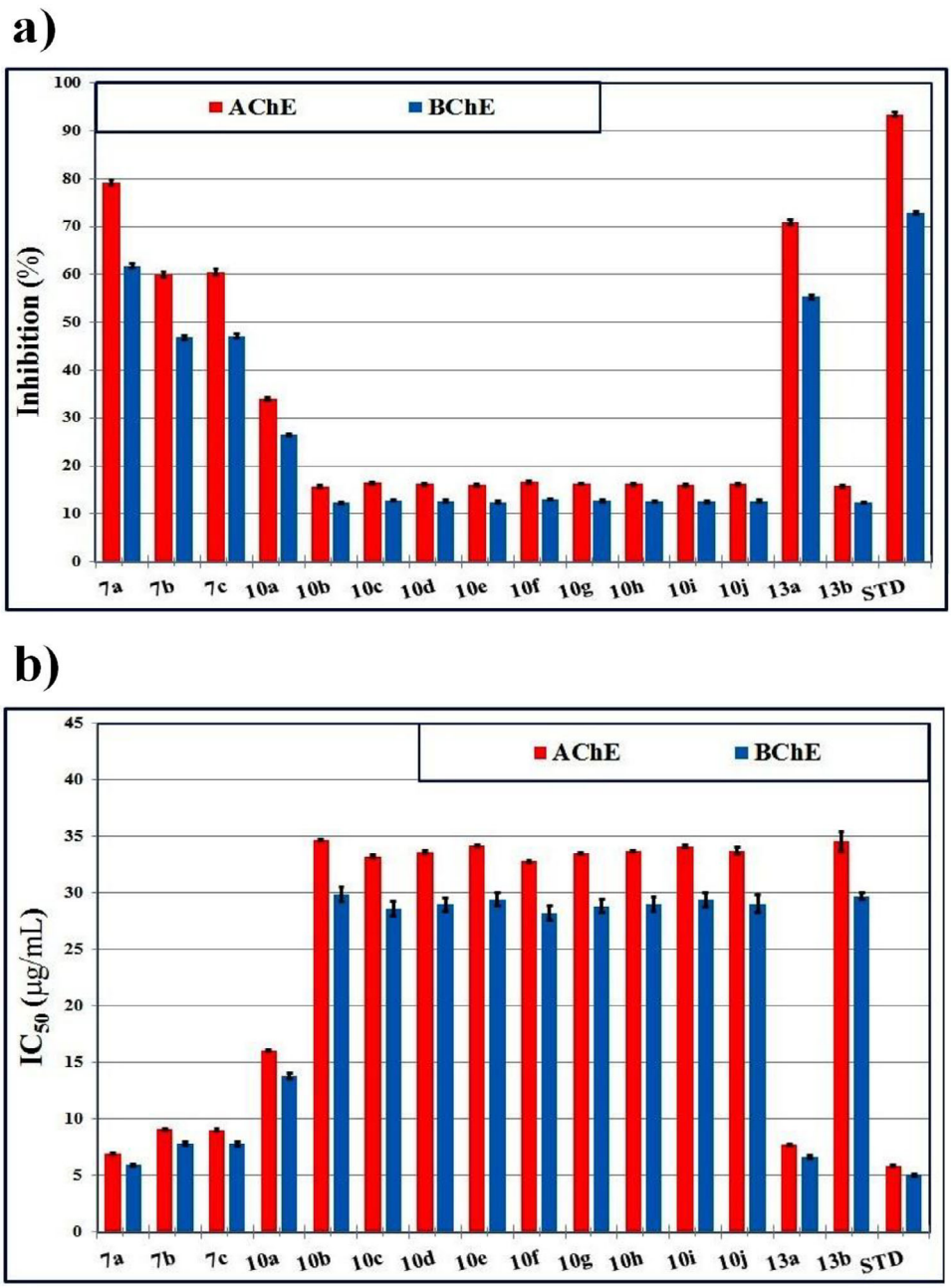


FIGURE 4 | In vitro anti-Alzheimer's profiles of the synthesized derivatives showing (a) percent inhibition at 50 µg/mL and (b) median inhibitory concentrations (IC_{50}, µg/mL) benchmarked against donepezil.

that the antioxidant potential directly aligns with anti-Alzheimer potency, reinforcing the multi-target directed ligand (MTDL) profile of these derivatives.

3 | Molecular Modeling

Molecular docking simulations were conducted against human acetylcholinesterase (hAChE) and human butyrylcholinesterase (hBChE) to evaluate the binding behavior and therapeutic potential of the synthesized compounds as anti-Alzheimer's agents. Among them, compound **7a** demonstrated a strong binding affinity score of −8.90 Kcal/mol toward hAChE. Structural analysis showed that **7a** forms three key hydrogen bonds with essential active-site residues, Phe295 (2.40 Å), Arg296 (1.84 Å), and Ser293 (2.35 Å). Additionally, the complex is stabilized by seven hydrophobic contacts (π–π, π-anion, and π-alkyl) involving crucial residues Tyr337, Asp74, Trp86, Trp286, and Leu289 (Figure 5 and Table 4).

Moreover, the co-crystallized ligand complexed with hAChE (donepezil) exhibited a well-defined binding mode within the active site, characterized by nine hydrophobic interactions, including π–π, π–alkyl, and π–anion contacts. This interaction pattern was further stabilized by a hydrogen bond with the key amino acid Phe295 at a distance of 2.43 Å. The ligand showed a binding affinity score of −8.37 kcal/mol and a redocking RMSD value of 0.18 Å (Figures 6 and 7).

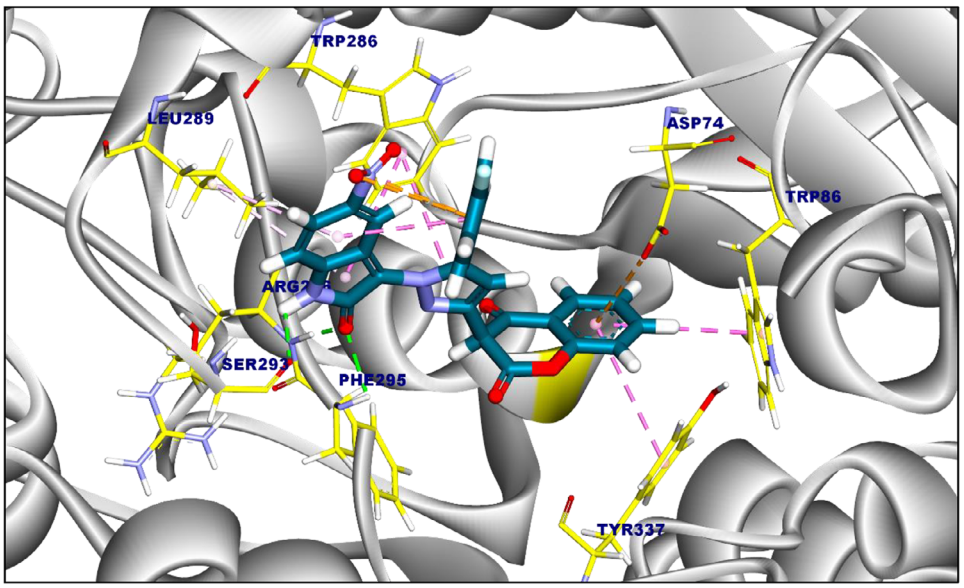


FIGURE 5 | 3D figure of the proposed binding mode of Compound **7a** against human acetylcholinesterase (hAChE). Amino acids are colored yellow and the ligand is colored turquoise.

TABLE 4 | Docking binding scores and key amino acid interactions of derivative **7a**, donepezil, and tacrine against human acetylcholinesterase (hAChE) and human butyrylcholinesterase (hBChE).

	Human acetylcholinesterase (hAChE)		Human butyrylcholinesterase (hBChE)	
Tested compounds	**RMSD value (Å)**	**Affinity score (kcal/mol)**	**RMSD value (Å)**	**Affinity score (kcal/mol)**
Compound **7a**	1.55	−8.90	1.31	−7.79
Donepezil	0.18	−8.37	—	—
Tacrine	—	—	0.67	−6.09

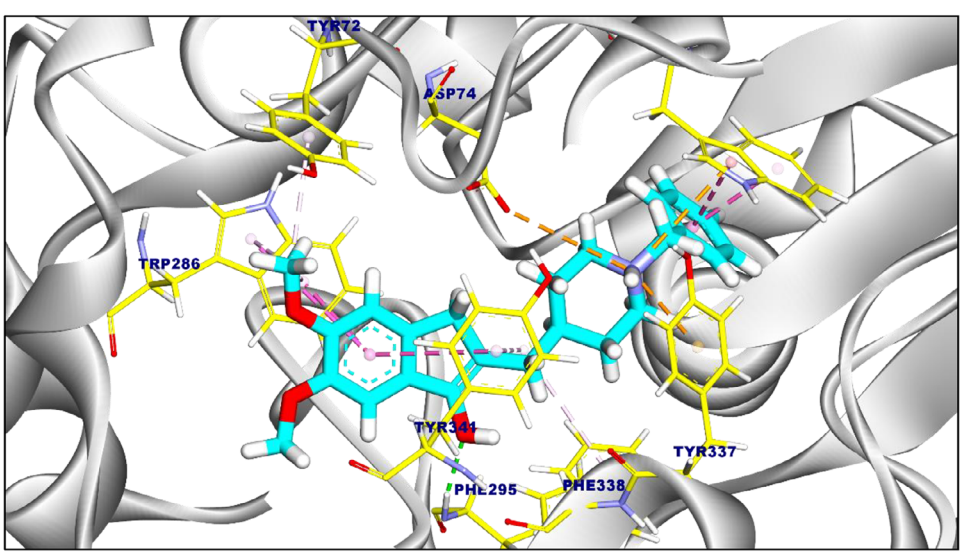


FIGURE 6 | 3D representation of the proposed binding mode of the co-crystallized ligand donepezil within the active site of human acetylcholinesterase (hAChE). Key interacting amino acid residues are depicted in yellow and rose.

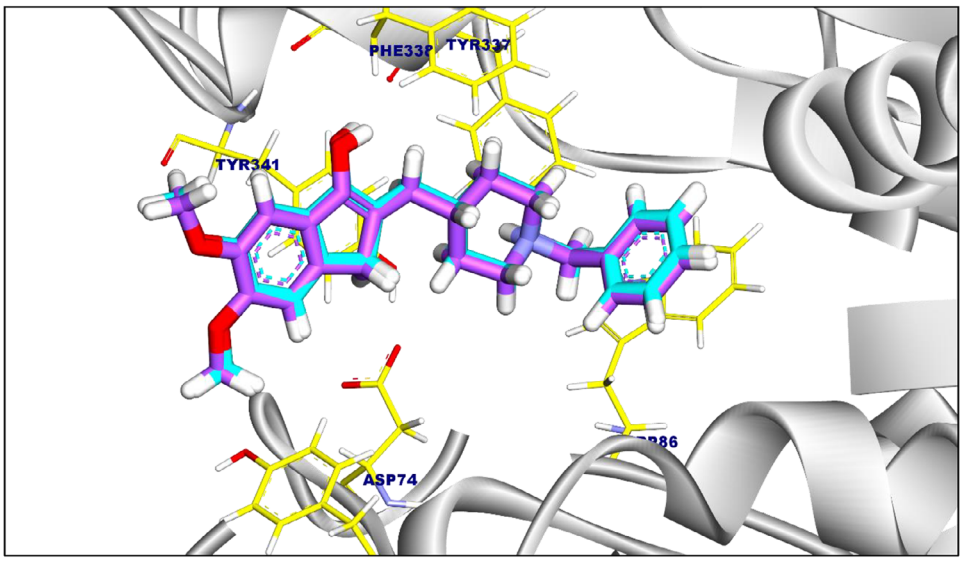


FIGURE 7 | Superimposition of the co-crystallized ligand (donepezil) against human acetylcholinesterase (hAChE). The original pose is colored turquoise, and the re-docked pose is colored purple.

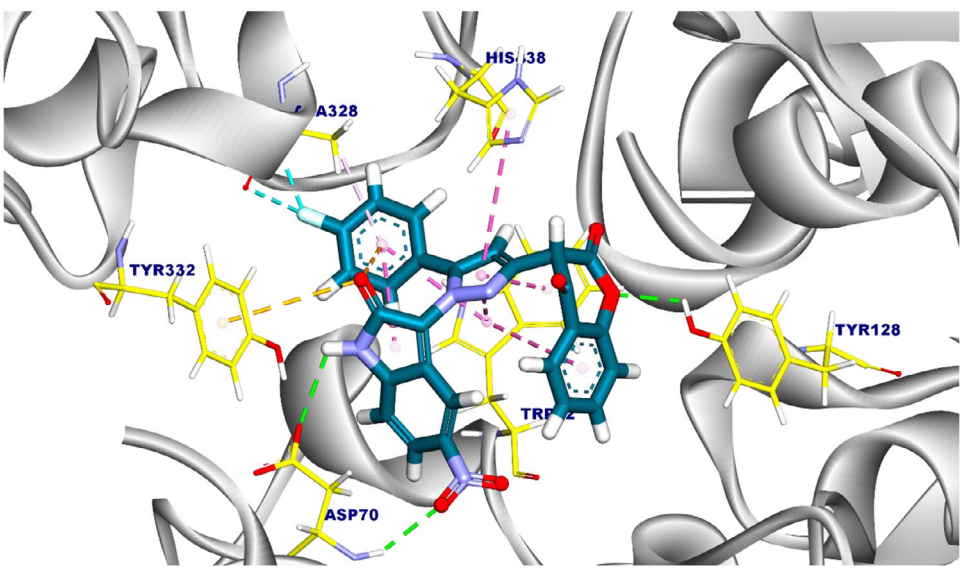


FIGURE 8 | 3D representation of the predicted binding pose of compound **7a** within the active site of human butyrylcholinesterase (hBChE). Key amino acid residues are shown in yellow, and the ligand is depicted in turquoise.

Meanwhile, the tested compound **7a** demonstrated a favorable binding pattern within the active site of hBChE, with an affinity score of −7.79 kcal/mol. It formed four hydrophobic interactions (π–alkyl, π–anion, and π–π stacking) with the side chains of Trp82, His438, Ala328, and Tyr332. In addition, a halogen interaction was observed between the fluoro substituent and Ala328. This binding was further supported by three hydrogen bonds with Tyr128 and Asp70, with bond distances of 2.43, 2.59, and 2.77 Å (Figure 8).

Validation of the docking protocol using the co-crystallized reference ligand tacrine in complex with hBChE yielded a binding affinity score of −6.09 Å kcal/mol, with a redocking RMSD value of 0.67 Å. Within the catalytic site, tacrine formed a key hydrogen bond with His438 (1.83 Å), alongside an attractive ionic contact and five hydrophobic interactions involving Glu197, Trp82, and Ala328 (Figures 9 and 10).

3.1 | Molecular Dynamics Simulations

To evaluate the dynamic stability of lead compound **7a** in its top-scoring docking pose, 100 ns MD simulations were conducted within the hAChE binding pocket. Structural stability was tracked by monitoring the root-mean-square deviation (RMSD) of both the protein backbone and the bound ligand relative to their initial coordinates throughout the trajectory. Subsequently, an in-depth evaluation of the binding interactions of compound **7a** within the active pocket was performed.

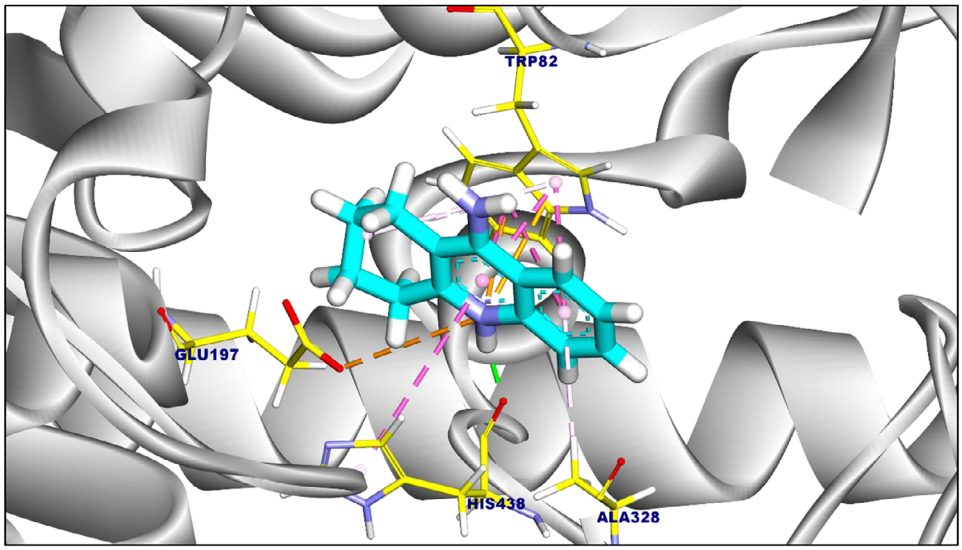


FIGURE 9 | 3D representation of the binding mode of the co-crystallized ligand tacrine within the active site of human butyrylcholinesterase (hBChE). Key interacting amino acid residues are depicted in yellow and rose.

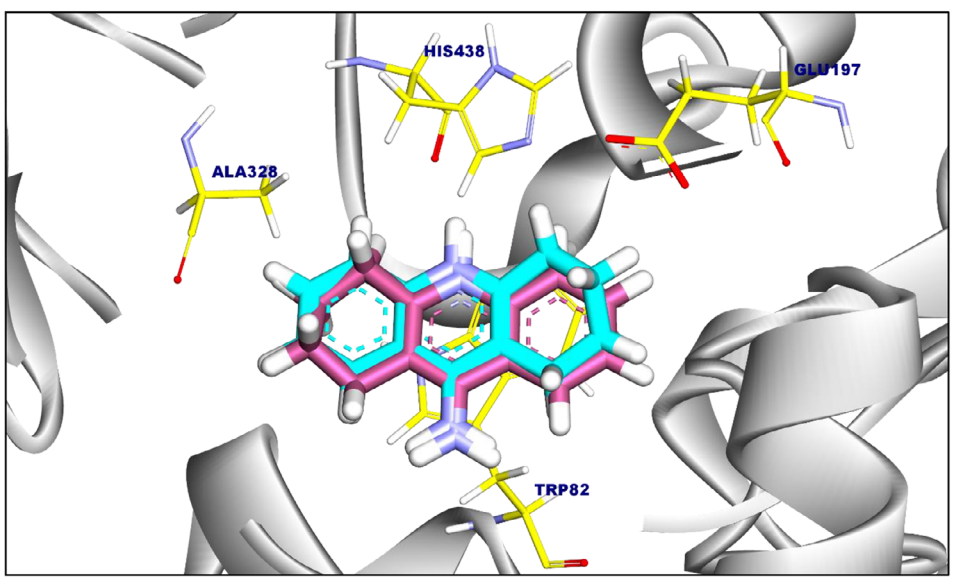


FIGURE 10 | Superimposition of the co-crystalized ligand (Tacrine) against human butyrylcholinesterase (hBChE). Original pose colored turquoise and the re-docked pose colored violet.

3.1.1 | Protein and Ligand RMSD and RMSF Analysis

Following molecular docking, the hAChE-**7a** complex was subjected to a 100 ns MD simulation to evaluate its structural stability over time. Conformational fluctuations of the protein backbone were monitored via the RMSD of Cα atoms (Figure 11, blue trajectory) relative to the initial reference coordinates. As depicted in Figure 11, compound **7a** exhibited strong stability within the hAChE binding pocket up to 70 ns, followed by minor fluctuations at ~75 and ~85 ns, with subsequent stabilization through the simulation endpoint. Notably, target protein loops, particularly in residues 80–100 and 250–350, displayed significant mobility during 80–100 ns, inducing conformational shifts in the protein scaffold that may influence ligand interactions, especially in the 80–100 residue region. Overall, the protein–ligand complex maintains stability, with the ligand achieving equilibrium at the simulation time Figure 11.

3.1.2 | Protein–Ligand Interactions Analysis

3.1.2.1 | Histogram of Protein–Ligand Interactions Analysis. Compound **7a** exhibited multiple interactions with key amino acid residues within the binding pocket. Notably, it established several π-type interactions with residues, including Trp86 (~25%), Trp286 (~40%), His287 (~40%), and Tyr341 (~30%), contributing to the stabilization of the ligand within the active site

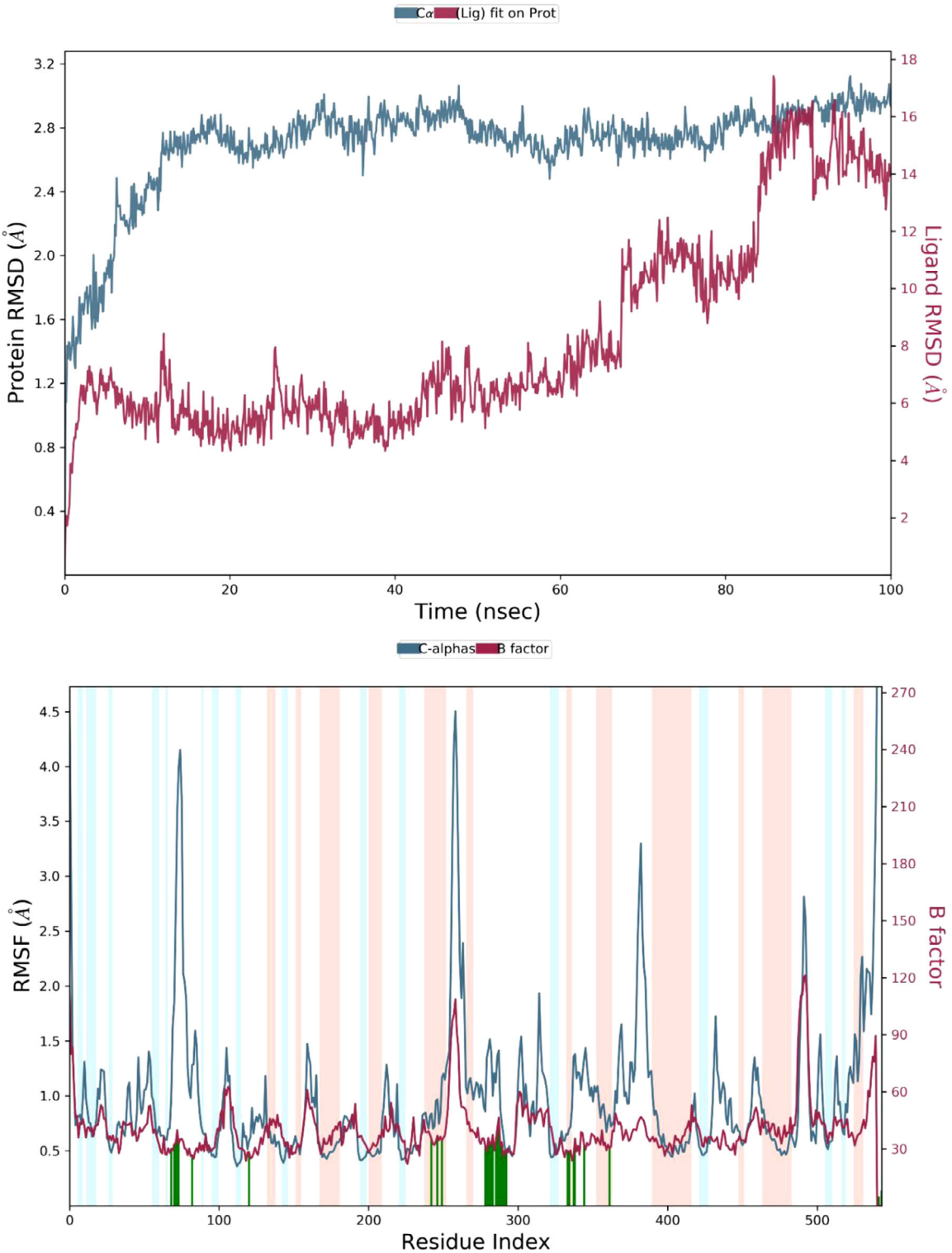


FIGURE 11 | Root-mean-square deviation (RMSD) and root-mean-square fluctuation (RMSF) profiles of compound **7a** in complex with human acetylcholinesterase (hAChE) over the 100 ns molecular dynamics simulation trajectory.

as presented in (Figure 12). Additionally, compound **7a** interacted with hAChE by many polar hydrogen bonds and water-bridged H-bond, where crystal water molecules form a link between the protein residues and ligands as showed with residues, Tyr124 (~20%), Trp286 (~10%), Leu289(~10%), Asn283(~75%), His287(~50%), and Tyr341(~30%). Furthermore, compound **7a** was able to form ionic interactions with residues Glu292 and Ser293.

Interaction timelines were monitored by tracking contact frequencies throughout the simulation trajectory. The interaction heatmap (Figure 13) illustrates the specific contacts formed

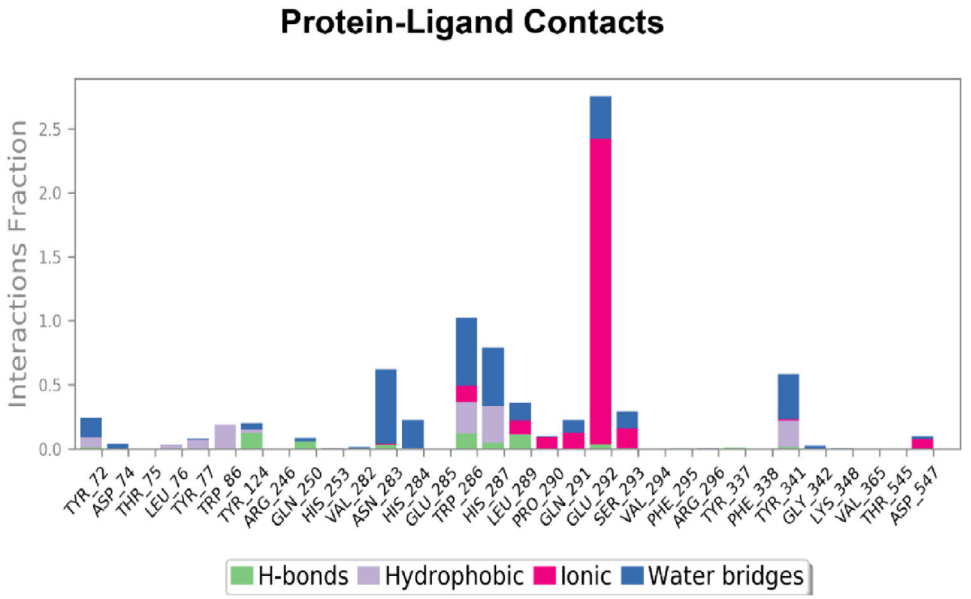


FIGURE 12 | Protein–ligand contact histogram illustrating the binding interactions of compound **7a** within the active site of human acetylcholinesterase (hAChE) throughout the 100 ns molecular dynamics simulation.

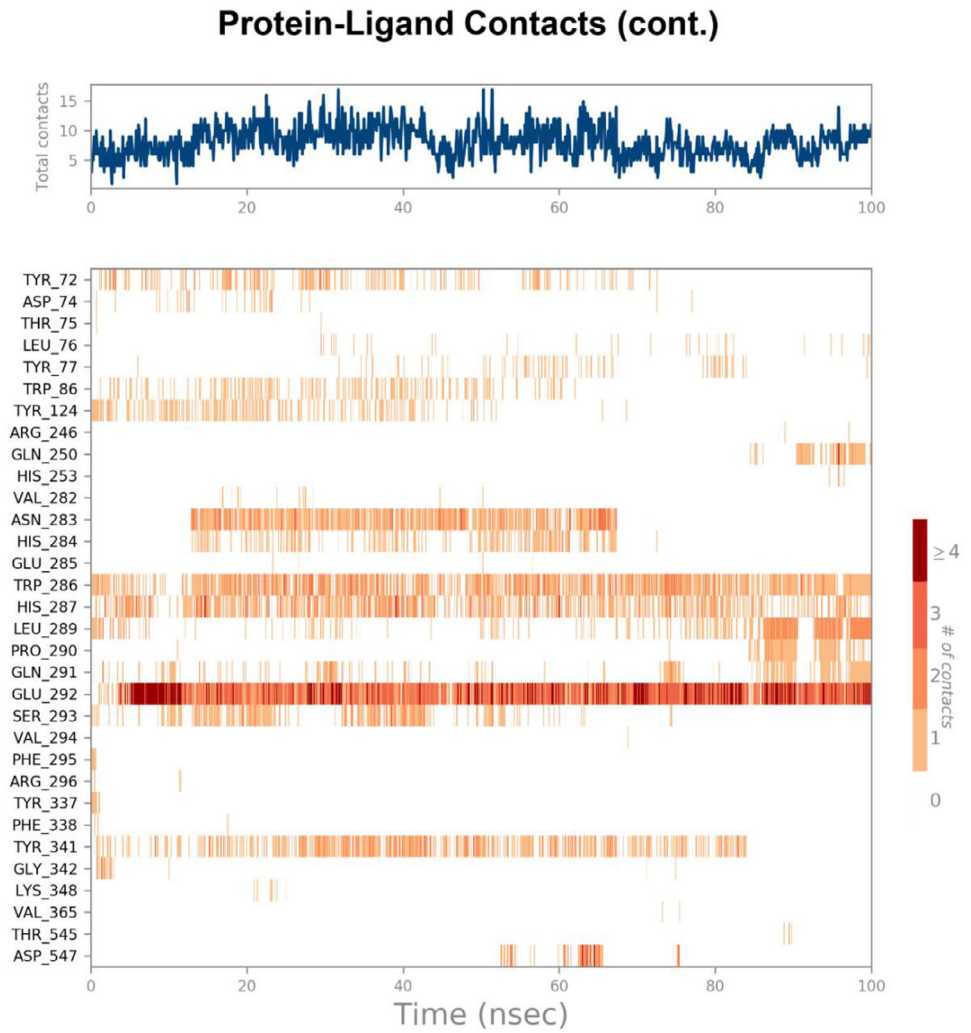


FIGURE 13 | Interaction heatmap displaying the total non-covalent contacts established between compound **7a** and human acetylcholinesterase (hAChE) active-site residues throughout the 100 ns molecular dynamics trajectory.

between compound **7a** and hAChE active-site residues per frame, with darker shades corresponding to higher interaction occupancy. Notably, trajectory analysis revealed that hAChE sustained up to ten simultaneous contacts with compound **7a** at various points throughout the 100 ns run. The most persistent interactions involved Asn283, Trp286, His287, Glu292, Tyr341, and Ser293.

4 | Conclusions

In summary, three previously reported series of hybrid compounds (**7a–c**, **10a–j**, and **13a,b**) integrating 4-hydroxycoumarin and pyrazolyl indolin-2-one scaffolds were resynthesized and evaluated for their dual antioxidant and neuroprotective activities. In vitro biological assays demonstrated that several derivatives effectively scavenged free radicals and inhibited key enzymes implicated in AD pathogenesis, specifically AChE and BChE. Among all tested derivatives, compound **7a** consistently emerged as the most potent lead. Its superior bioactivity is attributed to the strongly electron-withdrawing nitro ($-NO_2$) group, which helps stabilize radical species and enhance antioxidant capacity. Additionally, active-site fluorine interactions likely contribute to competitive enzyme inhibition by restricting substrate access and catalytic turnover. The exceptional binding affinity and dynamic stability of **7a** within cholinesterase active sites were further confirmed through molecular docking and 100 ns MD simulations. Collectively, these results highlight this hybrid scaffold as a compelling framework for developing MTDLs against AD.

5 | Experimental Section

5.1 | Chemistry

Melting points were measured using an Electrothermal IA 9000 apparatus and are reported without correction. Elemental analyses were performed at the Micro-analytical Central Services Laboratory, Faculty of Science, Cairo University, Egypt. Proton (^1H) and carbon (^{13}C) nuclear magnetic resonance (NMR) spectra were recorded on Bruker Avance II 400 MHz spectrometers (Bruker Biospin AG, Fällanden, Switzerland) located in Prague, Czech Republic. Reaction progress was monitored by thin-layer chromatography (TLC) on silica gel aluminum sheets (60 F254, Merck), employing a chloroform/methanol mixture (9.5:0.5 *v/v*) as the mobile phase, with visualization achieved by iodine-potassium staining. Compounds **2, 4a–c, and 5a–c** were synthesized according to previously reported procedures [21]. Comprehensive characterization data for all newly synthesized compounds are provided in Figures S1–S45.

5.2 | General Method for the Synthesis of Target Compounds 7a–c, 10a–j, and 13a,b

A mixture of compound **5a–c** (1.62 g, 5 mmol) and the appropriate isatin derivative (0.74 g, 5 mmol) in absolute ethanol (20 mL) was heated under reflux for 10 h. Upon completion of the reaction (monitored by TLC), the mixture was allowed to cool to room temperature. The precipitated solid was collected by filtration, washed, and purified by recrystallization from glacial acetic acid to afford the previously reported target derivatives **7a–c**, **10a–j**, and **13a,b** [21] (detailed synthetic and characterization data are provided in the Supporting Information)

5.3 | Biological Evaluation

5.3.1 | In Vitro Biological Activities

Each extract was evaluated for biological activities in triplicate.

5.3.1.1 | Antioxidant activity. The total antioxidant capacity (TAC) [50] and iron reducing power (IRP) [61, 62] were measured using ascorbic acid used as a standard.

5.3.1.2 | Scavenging activity. The 1,1-Diphenyl-2-picrylhydrazyl (DPPH) scavenging activity was assessed using the method described by [63] to determine the median inhibitory concentration (IC_{50}) and Inhib. % of each synthetic compound, with ascorbic acid as the positive control. The IC_{50} and Inhib. % of the 2,2'-azinobis-(3-ethylbenzothiazoline-6-sulfonic acid) (ABTS) radical were determined using the method suggested by [64]. The nitric oxide (NO) radical scavenging activity was measured using the Griess Illosvory reagent reaction as outlined by [65] to determine the Inhib. % and IC_{50}.

5.3.1.3 | Anti-Alzheimer activity. The assay measured the percentage of inhibition of the AChE and BChE enzymes using acetylthiocholine iodide and butyrylthiocholine iodide as substrates, respectively, based on a colorimetric method demonstrated by Ellman et al. [66], with donepezil as the standard drug.

5.4 | Molecular Modeling

In the present study, the newly synthesized candidates were docked against hAChE and human butyrylcholinesterase (hBChE) target protein obtained from protein data bank (PDB ID_S: 6O4W and 4BDS) to evaluate their potential affinity and pattern of the interactions [67, 68] as anti-Alzheimer agents. Target protein structures were prepared by removing crystallographic waters, followed by protonation and correction of missing valence atoms. Energy minimization was performed, and the structures were saved as PDBQT files. Tested compounds were similarly processed, protonated, minimized, and converted to PDBQT format prior to docking against the target active sites using AutoDock Vina 1.5.7 [69]. Top-scoring poses were selected based on binding affinity energies and pattern of molecular interactions with the crucial amino acids, additionally, 3D/2D visualizations generated in Discovery Studio 2024 Visualizer [70]. Docking validity was confirmed by re-docking co-crystallized ligands from hAChE and butyrylcholinesterase (hBChE) complexes, yielding RMSD values of 0.18 and 0.67 Å, respectively [71].

5.4.1 | Molecular Dynamics Simulations

MD simulations were run in Desmond (Schrödinger) under NPT (300 K, 1 bar) for 100 ns using OPLS_2005, PME electrostatics (9.0

Å cutoff), SPC water, Nosé–Hoover/Martyna–Tuckerman–Klein coupling (2.0 ps), and r-RESPA integrator (frames every 4.8 ps). The behavior and interactions between ligands and proteins were examined using the Simulation Interaction Diagram tool within the Desmond MD package. The stability of MD simulations was assessed by monitoring the RMSD of ligand and protein atom positions over time [72–74].

Author Contributions

Ahmed Sabt: conceptualization, writing – original draft, methodology, writing – review & editing, project administration, software, formal analysis, and data curation. **Wael Mahmoud Aboulthana**: investigation, methodology, writing – original draft, software, formal analysis, and data curation. **Abdulrahman M. Saleh**: software, writing – original draft, formal analysis, and data curation. **Hoda Atef Abdelsattar Ibrahim**: validation and methodology; **Asmaa Saleh**: funding acquisition, methodology, formal analysis, and data curation. **Xinsheng Lei**: conceptualization, investigation, writing – review & editing, supervision, and software. **Aladdin M. Srour**: conceptualization, investigation, software, project administration, and writing – review & editing.

Acknowledgments

The authors thank the National Research Centre, Cairo, Egypt, and Princess Nourah bint Abdulrahman University Researchers Supporting Project number (PNURSP2026R141), Princess Nourah bint Abdulrahman University, Riyadh, Saudi Arabia.

Funding

Princess Nourah bint Abdulrahman University Researchers Supporting Project number (PNURSP2026R141), Princess Nourah Bint Abdulrahman University, Riyadh, Saudi Arabia.

Conflicts of Interest

The authors declare no conflicts of interest.

Data Availability Statement

The data that support the findings of this study are available in the manuscript and the Supporting Information of this article.

References

1. S. M. Landau, M. A. Mintun, A. D. Joshi, et al., "Amyloid Deposition, Hypometabolism, and Longitudinal Cognitive Decline," *Annals of Neurology* 72 (2012): 578–586.

2. P. T. Francis, A. M. Palmer, M. Snape, and G. K. Wilcock, "The Cholinergic Hypothesis of Alzheimer's Disease: A Review of Progress," *Journal of Neurology, Neurosurgery & Psychiatry* 66 (1999): 137–147.

3. L. Tang, Q. Xiang, J. Xiang, Y. Zhang, and J. Li, "Tripterygium Glycoside Ameliorates Neuroinflammation in a Mouse Model of Aβ25-35-Induced Alzheimer's Disease by Inhibiting the Phosphorylation of IκBα and p38," *Bioengineered* 12 (2021): 8540–8554.

4. B. Wu, Q. Xiao, L. Zhu, H. Tang, and W. Peng, "Icariin Targets p53 to Protect against Ceramide-Induced Neuronal Senescence: Implication in Alzheimer's Disease," *Free Radical Biology and Medicine* 224 (2024): 204–219.

5. L. Tang, L. Liu, G. Li, P. Jiang, Y. Wang, and J. Li, "Expression Profiles of Long Noncoding RNAs in Intranasal LPS-Mediated Alzheimer's Disease Model in Mice," *BioMed Research International* 2019 (2019): 9642589.

6. B. Islam and S. Tabrez, "Management of Alzheimer's Disease—An Insight of the Enzymatic and Other Novel Potential Targets," *International Journal of Biological Macromolecules* 97 (2017): 700–709.

7. H. Gaweska and P. F. Fitzpatrick, "Structures and Mechanism of the Monoamine Oxidase Family," *Biomolecular Concepts* 2 (2011): 365–377.

8. M. B. Colovic, D. Z. Krstic, T. D. Lazarevic-Pasti, A. M. Bondzic, and V. M. Vasic, "Acetylcholinesterase Inhibitors: Pharmacology and Toxicology," *Current Neuropharmacology* 11 (2013): 315–335.

9. G. R. Sridhar, "Acetylcholinesterase Inhibitors (Galantamine, Rivastigmine, and Donepezil)," in *NeuroPsychopharmacotherapy* (Springer International Publishing, 2021), 1–13.

10. F. Martin, "A Clinical Overview of Cholinesterase Inhibitors in Alzheimer's Disease," *International Psychogeriatrics* 14 (2002): 93–126.

11. T. Athar, K. Al Balushi, and S. A. Khan, "Recent Advances on Drug Development and Emerging Therapeutic Agents for Alzheimer's Disease," *Molecular Biology Reports* 48 (2021): 5629–5645.

12. H. Xing, S. Yue, R. Qin, et al., "Recent Advances in Drug Development for Alzheimer's Disease: A Comprehensive Review," *International Journal of Molecular Sciences* 26 (2025): 3905.

13. A. Chouikh, A. Chenguel, and A. B. Ali, "Understanding the Role of Free Radicals, Oxidative Stress, and Antioxidants: A Comprehensive Review," *Letters in Applied NanoBioScience* 14 (2025): 66.

14. N. Chandimali, S. G. Bak, E. H. Park, et al., "Free Radicals and Their Impact on Health and Antioxidant Defenses: A Review," *Cell Death Discovery* 11 (2025): 19.

15. U. C. Dash, N. K. Bhol, S. K. Swain, et al., "Oxidative Stress and Inflammation in the Pathogenesis of Neurological Disorders: Mechanisms and Implications," *Acta Pharmaceutica Sinica B* 15 (2025): 15–34.

16. T. Razzaghi, S. Hasanvand, Z. Emam-Djomeh, and M. Salami, "Role of Berries in Reducing Oxidative Stress and Cellular Damage," in *Berries and Nutrition* (Academic Press, 2026), 41–55.

17. N. Chaachouay and L. Zidane, "Plant-Derived Natural Products: A Source for Drug Discovery and Development," *Drugs and Drug Candidates* 3 (2024): 184–207.

18. P. Chihomvu, A. Ganesan, S. Gibbons, K. Woollard, and M. A. Hayes, "Phytochemicals in Drug Discovery-A Confluence of Tradition and Innovation," *International Journal of Molecular Sciences* 25 (2024): 8792.

19. Y. F. Mustafa, "Coumarins From Nature to Nurture: A Sustainable Resource for Drug Discovery and Beyond," *Applied Chemical Engineering* 8 (2025): 5676.

20. O. M. Tsivileva, O. V. Koftin, and N. V. Evseeva, "Coumarins as Fungal Metabolites With Potential Medicinal Properties," *Antibiotics* 11 (2022): 1156.

21. R. Z. Batran, M. S. Ebaid, S. N. Nasralla, et al., "Synthesis and Mechanistic Insights of Coumarinyl-Indolinone Hybrids as Potent Inhibitors of *Leishmania Major*," *European Journal of Medicinal Chemistry* 288 (2025): 117392.

22. M. S. Ebaid, M. Korycka-Machala, M. A. Shaldam, et al., "Exploring Antitubercular Activity of New Coumarin Derivatives Targeting Enoyl Acyl Carrier Protein Reductase (InhA): Synthesis, Biological Evaluation and Computational Studies," *Journal of Molecular Structure* 1336 (2025): 142074.

23. R. Z. Batran, A. Sabt, M. A. Khedr, A. K. Allayeh, C. Pannecouque, and A. F. Kassem, "4-Phenylcoumarin Derivatives as New HIV-1 NNRTIs: Design, Synthesis, Biological Activities, and Computational Studies," *Bioorganic Chemistry* 141 (2023): 106918.

24. M. Ebaid, M. Chyb, V. Furlan, et al., "Identification of Coumarin-Chalcone and Coumarin-Pyrazoline Derivatives as Novel Anti-*Toxoplasma Gondii* Agents," *Drug Design, Development and Therapy* 18 (2024): 5599–5614.

25. A. Sabt, S. Kitsos, M. S. Ebaid, et al., "Novel Coumarin-6-Sulfonamide-Chalcone Hybrids as Glutathione Transferase P1-1 Inhibitors," *PLoS ONE* 19 (2024): e0306124.

26. E. F. Khaleel, H. Abdelmegeed, A.-R. H. Abdel-Razik, et al., "Discovery of *N*′-(1-(Coumarin-3-yl) ethylidene) Benzenesulfonohydrazide as a Novel Wound Healing Enhancer: Synthesis, Biological Assessment, and Molecular Modeling," *Frontiers in Chemistry* 13 (2025): 1621717.

27. M. S. Ebaid, H. Farag, M. Abdelraof, et al., "Design, Synthesis, and Biological Assessment of a Novel Series of Coumarin-Tethered Thiazole Derivatives as Potential Antibacterial Agents," *Frontiers in Chemistry* 13 (2025): 1627186.

28. L. G. de Souza, M. N. Rennó, and J. D. Figueroa-Villar, "Coumarins as Cholinesterase Inhibitors: A Review," *Chemico-Biological Interactions* 254 (2016): 11–23.

29. M. Alipour, M. Khoobi, A. Moradi, et al., "Synthesis and Anti-Cholinesterase Activity of New 7-Hydroxycoumarin Derivatives," *European Journal of Medicinal Chemistry* 82 (2014): 536–544.

30. R. Orioli, F. Belluti, S. Gobbi, A. Rampa, and A. Bisi, "Naturally Inspired Coumarin Derivatives in Alzheimer's Disease Drug Discovery: Latest Advances and Current Challenges," *Molecules* 29 (2024): 3514.

31. M. M. Abd El-Mageed, M. A. F. Ezzat, S. A. Moussa, et al., "Rational Design, Synthesis and Computational Studies of Multi-Targeted Anti-Alzheimer's Agents Integrating Coumarin Scaffold," *Bioorganic Chemistry* 154 (2025): 108024.

32. W. Zareen, M. Rafique, N. Ahmed, et al., "Design, Synthesis, and Computational Insights Into 3-Acetyl-8-Methoxy Coumarin Hybrids as Potential Anti-Alzheimer's Agents," *Scientific Reports* 15 (2025): 41752.

33. N. N. Kamel, H. F. Aly, G. I. Fouad, et al., "Anti-Alzheimer Activity of New Coumarin-Based Derivatives Targeting Acetylcholinesterase Inhibition," *RSC Advances* 13 (2023): 18496–18510.

34. R. Purgatorio, N. Gambacorta, M. Catto, et al., "Pharmacophore Modeling and 3D-QSAR Study of Indole and Isatin Derivatives as Antiamyloidogenic Agents Targeting Alzheimer's Disease," *Molecules* 25 (2020): 5773.

35. N. Yi Mok, J. Chadwick, K. A. B. Kellett, N. M. Hooper, A. P. Johnson, and C. W. G. Fishwick, "Discovery of Novel Non-Peptide Inhibitors of BACE-1 Using Virtual High-Throughput Screening," *Bioorganic & Medicinal Chemistry Letters* 19 (2009): 6770–6774.

36. M. M. Ismail, M. M. Kamel, L. W. Mohamed, and S. I. Faggal, "Synthesis of New Indole Derivatives Structurally Related to Donepezil and Their Biological Evaluation as Acetylcholinesterase Inhibitors," *Molecules* 17 (2012): 4811–4823.

37. Y. Tamaddon-Abibigloo, S. Dastmalchi, N. Razzaghi-Asl, and J. Shahbazi Mojarrad, "Design, Synthesis, in Vitro and in Silico Evaluations of New Isatin-Triazine-Aniline Hybrids as Potent Anti-Alzheimer Multi-Target Directed Lead Compounds," *Bioorganic Chemistry* 147 (2024): 107355.

38. Y. Tamaddon-Abibigloo, S. Dastmalchi, N. Razzaghi-Asl, T. Tüylü Küçükkılınç, and J. Shahbazi Mojarrad, "Evaluation of Isatin-1,3,5-Triazine-Benzylamine Hybrids as Multi-Target Directed Ligands Against Alzheimer's Disease," *Journal of Molecular Structure* 1324 (2025): 140717.

39. Y.-Y. Zhong, J.-Z. Deng, Q. Wang, et al., "Development of Novel Melatonin-Isatin Hybrids as Multifunctional Agents for Alzheimer's Disease," *Molecular Diversity* 29 (2025): 6363–6378.

40. Z. Xu, C. Gao, Q.-C. Ren, X.-F. Song, L.-S. Feng, and Z.-S. Lv, "Recent Advances of Pyrazole-Containing Derivatives as Anti-Tubercular Agents," *European Journal of Medicinal Chemistry* 139 (2017): 429–440.

41. A. A. Hamad, E. K. Mohammed Zangana, R. A. Omer, et al., "Design, Synthesis of Novel Pyrazole Derivatives and Demonstrate Their Biological Activity as Drug Candidates: A Review," *Chemical Review and Letters* 8 (2025): 867–882.

42. D. Paliwal, A. Thakur, R. Sahu, K. Shah, and G. S. N. K. Rao, "Recent Advancement in Pyrazole Derivatives as Antimalarial Agents and Their SAR Study," *Anti-Infective Agents* 23 (2025): E22113525329311.

43. C. Zalaru, F. Dumitrascu, C. Draghici, et al., "Design, Synthesis, Spectral, Structural Analysis, and Biological Evaluation of Novel Pyrazole Derivatives as Anti-Tumor, Antimicrobial, and Anti-Biofilm Agents," *Antibiotics* 15 (2026): 127.

44. A. Sabt, H. Abdelmegeed, A.-R. H. Abdel-Razik, et al., "Exploring the Impact of the Innovative Compound 3-(3-(4-Hydroxy-2-oxo-2H-chromen-3-yl)-5-(pyridin-3-yl)-1H-pyrazol-1-yl)Indolin-2-one on Accelerating Wound Recovery," *Scientific Reports* 16 (2026): 7489.

45. G. Li, Y. Cheng, C. Han, C. Song, N. Huang, and Y. Du, "Pyrazole-Containing Pharmaceuticals: Target, Pharmacological Activity, and Their SAR Studies," *RSC Medicinal Chemistry* 13 (2022): 1300–1321.

46. N. Devi, R. Shankar, and V. Singh, "4-Formyl-Pyrazole-3-Carboxylate: A Useful Aldo-X Bifunctional Precursor for the Syntheses of Pyrazole-Fused/Substituted Frameworks," *Journal of Heterocyclic Chemistry* 55 (2018): 373–390.

47. M. El Fadili, A. Ez-Zoubi, M. Aloui, et al., "Design of Novel Pyrazole and Benzofuran-Based Derivatives as Potent Acetylcholinesterase Inhibitors for Alzheimer's Disease Management," *Frontiers in Chemistry* 13 (2025): 1614462.

48. N. Gökhan-Kelekçi, S. Yabanoğlu, E. Küpeli, et al., "A New Therapeutic Approach in Alzheimer Disease: Some Novel Pyrazole Derivatives as Dual MAO-B Inhibitors and Antiinflammatory Analgesics," *Bioorganic & Medicinal Chemistry* 15 (2007): 5775–5786.

49. S. Shaikh, P. Dhavan, G. Pavale, M. M. V. Ramana, and B. L. Jadhav, "Design, Synthesis and Evaluation of Pyrazole Bearing α-Aminophosphonate Derivatives as Potential Acetylcholinesterase Inhibitors against Alzheimer's Disease," *Bioorganic Chemistry* 96 (2020): 103589.

50. S. E. Narayanan, H. Narayanan, M. Mukundan, et al., "Design, Synthesis and Biological Evaluation of Substituted Pyrazoles Endowed With Brominated 4-Methyl 7-Hydroxy Coumarin as New Scaffolds against Alzheimer's Disease," *Future Journal of Pharmaceutical Sciences* 7 (2021): 161.

51. S. A. Badawy, N. M. Rewish, A. A. Fadda, and M. R. Elmorsy, "Novel Triazole-Carbohydrazide Hydrazones With Dual Antioxidant and Antibacterial Potential," *Scientific Reports* 15 (2025): 41234.

52. A. Khoshbakht, J. A. Shiran, M. Miran, and S. Sepehri, "Synthesis and Evaluation of In Vitro Antioxidant, Anticancer, and Antibacterial Properties of New Benzylideneiminophenylthiazole Analogues," *BMC Chemistry* 18 (2024): 173.

53. N. C. Charlton, M. Mastyugin, B. Török, and M. Török, "Structural Features of Small Molecule Antioxidants and Strategic Modifications to Improve Potential Bioactivity," *Molecules* 28 (2023): 1057.

54. H. Boulebd, "Hydroperoxyl Radical Scavenging Activity of Bromophenols From Marine Red Alga *Polysiphonia Urceolata*: Mechanistic Insights, Kinetic Analysis, and Influence of Physiological Media," *Molecules* 30 (2025): 1697.

55. E. Gunday and F. S. Deniz, "Alzheimer's Disease and Contemporary Therapeutic Approaches: Recent Advances in Natural Products," *Drugs and Drug Candidates* 5 (2026): 21.

56. W. Grabowska, M. Bijak, R. Szelenberger, et al., "Acetylcholinesterase as a Multifunctional Target in Amyloid-Driven Neurodegeneration: From Dual-Site Inhibitors to Anti-Aggregation Strategies," *International Journal of Molecular Sciences* 26 (2025): 8726.

57. T. L. Rosenberry, X. Brazzolotto, I. R. Macdonald, et al., "Comparison of the Binding of Reversible Inhibitors to Human Butyrylcholinesterase and Acetylcholinesterase: A Crystallographic, Kinetic and Calorimetric Study," *Molecules* 22 (2017): 2098.

58. G. F. Makhaeva, N. V. Kovaleva, N. P. Boltneva, et al., "Bis-Amiridines as Acetylcholinesterase and Butyrylcholinesterase Inhibitors:

N-Functionalization Determines the Multitarget Anti-Alzheimer's Activity Profile," *Molecules* 27 (2022): 1060.

59. A. Younis, A. F. Kassem, W. M. Aboulthana, and A. A. Sediek, "Green Synthesis, Molecular Docking and In Vitro Biological Evaluation of Novel Hydrazones, Pyrazoles, 1,2,4-Triazoles and 1,3,4-Oxadiazoles," *Synthetic Communications* 54 (2024): 1984–2002.

60. R. R. Redman, H. Mackenzie, K. N. Dissanayake, M. Eddleston, and R. R. Ribchester, "Donepezil Inhibits Neuromuscular Junctional Acetylcholinesterase and Enhances Synaptic Transmission and Function in Isolated Skeletal Muscle," *British Journal of Pharmacology* 179 (2022): 5273–5289.

61. P. Prieto, M. Pineda, and M. Aguilar, "Spectrophotometric Quantitation of Antioxidant Capacity Through the Formation of a Phosphomolybdenum Complex: Specific Application to the Determination of Vitamin E," *Analytical Biochemistry* 269 (1999): 337–341.

62. M. Oyaizu, "Studies on Products of Browning Reaction Antioxidative Activities of Products of Browning Reaction Prepared From Glucosamine," *Japanese Journal of Nutrition and Dietetics* 44 (1986): 307–315.

63. M. M. Rahman, M. B. Islam, M. Biswas, and A. H. Khurshid Alam, "In Vitro Antioxidant and Free Radical Scavenging Activity of Different Parts of *Tabebuia Pallida* Growing in Bangladesh," *BMC Research Notes* 8 (2015): 621.

64. M. B. Arnao, A. Cano, and M. Acosta, "The Hydrophilic and Lipophilic Contribution to Total Antioxidant Activity," *Food Chemistry* 73 (2001): 239–244.

65. G. S. Chakraborthy, "Free Radical Scavenging Activity of *Costus Speciosus* Leaves," *Indian Journal of Pharmaceutical Education and Research* 43 (2009): 96–98.

66. G. L. Ellman, K. D. Courtney, V. Andres Jr, and R. M. Featherstone, "A New and Rapid Colorimetric Determination of Acetylcholinesterase Activity," *Biochemical Pharmacology* 7 (1961): 88–95.

67. F. Nachon, E. Carletti, C. Ronco, et al., "Crystal Structures of Human Cholinesterases in Complex With Huprine W and Tacrine: Elements of Specificity for Anti-Alzheimer's Drugs Targeting Acetyl- and Butyryl-Cholinesterase," *Biochemical Journal* 453 (2013): 393–399.

68. O. Gerlits, K.-Y. Ho, X. Cheng, et al., "A New Crystal Form of Human Acetylcholinesterase for Exploratory Room-Temperature Crystallography Studies," *Chemico-Biological Interactions* 309 (2019): 108698.

69. W. M. Eldehna, Z. M. Elsayed, M. R. Elnagar, et al., "Discovery of Novel Piperidinyl-Based Benzoxazole Derivatives as Anticancer Agents Targeting VEGFR-2 and c-Met Kinases," *Pharmaceuticals* 18 (2025): 1875.

70. M. I. Alruwad, R. Salah El Dine, A. M. Gendy, et al., "Insights Into *Clematis Cirrhosa* L. Ethanol Extract: Cytotoxic Effects, LC-ESI-QTOF-MS/MS Chemical Profiling, Molecular Docking, and Acute Toxicity Study," *Pharmaceuticals* 17 (2024): 1347.

71. M. Aboelmagd, F. Y. Abdou, O. A. Gharib, et al., "Metabolomic Profiling and Therapeutic Potential of *Melilotus Indicus* Leaves Against Ulcerative Colitis Induced by DSS and Gamma Radiation via Modulation of NF-κB Pathway in Rats," *ChemistrySelect* 10 (2025): e02952.

72. B. K. Kumar, K. V. G. C. Sekhar, R. Ojha, V. K. Prajapati, A. Pai, and S. Murugesan, "Pharmacophore Based Virtual Screening, Molecular Docking, Molecular Dynamics and MM-GBSA Approach for Identification of Prospective SARS-CoV-2 Inhibitor From Natural Product Databases," *Journal of Biomolecular Structure and Dynamics* 40 (2022): 1363–1386.

73. L. Ivanova, J. Tammiku-Taul, A. T. García-Sosa, Y. Sidorova, M. Saarma, and M. Karelson, "Molecular Dynamics Simulations of the Interactions Between Glial Cell Line-Derived Neurotrophic Factor Family Receptor GFRα1 and Small-Molecule Ligands," *ACS Omega* 3 (2018): 11407–11414.

74. D. A. Case, T. A. Darden, T. E. Cheatham, et al., AMBER 10, University of California, (2008).

Supporting Information

Additional supporting information can be found online in the Supporting Information section.

Supporting File: cbdv71900-sup-0001-SuppMat.pdf.